Detailed fine structure of x-ray magnetic circular dichroism spectra: Systematics for heavy rare-earth magnets

C. Sorg,* A. Scherz,† K. Baberschke, and H. Wende
Institut für Experimentalphysik, Freie Universität Berlin, Arnimallee 14, D-14195 Berlin-Dahlem, Germany

F. Wilhelm and A. Rogalev
European Synchrotron Radiation Facility (ESRF), BP 220, 38043 Grenoble, France

S. Chadov, J. Minár, and H. Ebert
Department Chemie und Biochemie, Physikalische Chemie, Universität München, Butenandtstrasse 5-13, D-81377 München, Germany
(Received 26 September 2006; revised manuscript received 22 November 2006; published 28 February 2007)

X-ray absorption spectroscopy (XAS) and x-ray magnetic circular dichroism (XMCD) have been investigated at the $L_{2,3}$ edges of three heavy rare-earth elementary metals. In addition the XAS and XMCD spectra were calculated using a fully relativistic multiple scattering or Korringa-Kohn-Rostoker formalism. This allows disentanglement of electric dipole and electric quadrupolar transitions and serves for a better understanding of the details of the spectroscopic fine structure.

DOI: 10.1103/PhysRevB.75.064428 PACS number(s): 78.70.Dm, 71.20.Eh

I. INTRODUCTION

Circularly polarized x-rays have become a powerful tool for investigating fundamental properties of ferromagnetic materials. Taking advantage of the x-ray magnetic circular dichroism (XMCD) technique the element-specific magnetism of bulk alloys and magnetic nanostructures is revealed. In particular, XMCD at the $L_{2,3}$ edges is commonly used to study the orbital and spin moments of the heavy $3d$ elements Fe, Co, and Ni.[1,2]

In this work we present the systematics of the x-ray absorption and XMCD of Gd, Tb, and Dy as representatives of the heavy lanthanides at their $L_{2,3}$ edges. Interpretation of XMCD at the $L_{2,3}$ edges of rare-earth elements is a matter of discussion since the first spectra have been presented.[3] These elements are characterized by their partly, but more than half-filled $4f$ shell. Their large magnetic moment arises mostly from the highly localized $4f$ orbitals which have very weak overlap with neighboring sites. The exchange interaction between the $4f$ electrons is mediated by the polarization of the $5d$ conduction band.[4] Since XMCD spectroscopy is a shell-selective method for magnetic measurements it provides a useful tool for studying the $5d$ magnetism directly and separately from the $4f$ magnetism. Electric dipole ($E1$) transitions occur to unoccupied states of the $5d$ band whereas electric quadrupolar ($E2$) transitions probe the $4f$ states. For the x-ray absorption at the $L_{2,3}$ edges of the lanthanides $E2$ transitions get quite important because the dipole approximation is not justified in the corresponding energy range.[5] The importance of $E2$ contributions to the XMCD is enhanced in addition by the fact that the spin-dependent spectral weight of the $4f$ final states is much higher than that of the $5d$ final states. Additional features in the XMCD due to $E2$ contributions appear at the low energy side of the edge, because the $E2$ transitions appear lower in energy than the $E1$ transitions. The core hole potential attracts the $4f$ stronger than the $5d$ ones and shifts the $E2$ peak below the edge.[6] Most of the XMCD data of rare-earth elements available up to now stem from measurements of compounds, e.g., Refs. 7–11. These compounds are in general complex structures including various interactions and hybridization between the different constituents. This may well introduce additional complication in the fine structure of the spectra. Therefore, we focused our measurements on single crystals of the pure metals. At the helical undulator beamlines of today's third generation synchrotrons XMCD spectra are obtained with a high energy resolution and an excellent signal-to-noise ratio yielding a detailed fine structure. Previous results on Tb at low temperature ($T \approx 4$ K) are discussed in Refs. 12 and 13. Here, we present a systematic study of the XMCD for the three heavy lanthanides Gd, Tb, and Dy in a large temperature range from ~4 K up to above the magnetic transition temperature. As we demonstrate below the XMCD for these elements exhibits a detailed fine structure. The question arises how this fine structure can be explained. Contrary to earlier works that had to make use of a phenomenological description of the dichroism at the $L_{2,3}$ edges of the rare earths,[14] we present *ab initio* calculations based on spin-density functional theory here. Within this framework we go beyond the earlier analyses of Ref. 14 and explicitly calculate for instance the spin dependence of the transition matrix elements which is responsible for the determination of the wrong sign of the $5d$ moment by means of the standard XMCD sum rule analysis.[15] Performing *ab initio* calculations as presented in the present paper has the advantage that individual transitions like $E1$or $E2$ can be turned on/off and therefore these features can be directly related to specific fine structures in the dichroic spectra. We find the resulting theoretical spectra to be in rather satisfying agreement with experiment providing a fundamental understanding of the spectroscopy itself. This supplies a very valuable support for the interpretation of the experimental spectra that can be decomposed into their $E1$ and $E2$ parts in an indirect way only.

II. EXPERIMENT

At room temperature all three elements have a hexagonal closed packed (hcp) structure. The crystals are cut such that

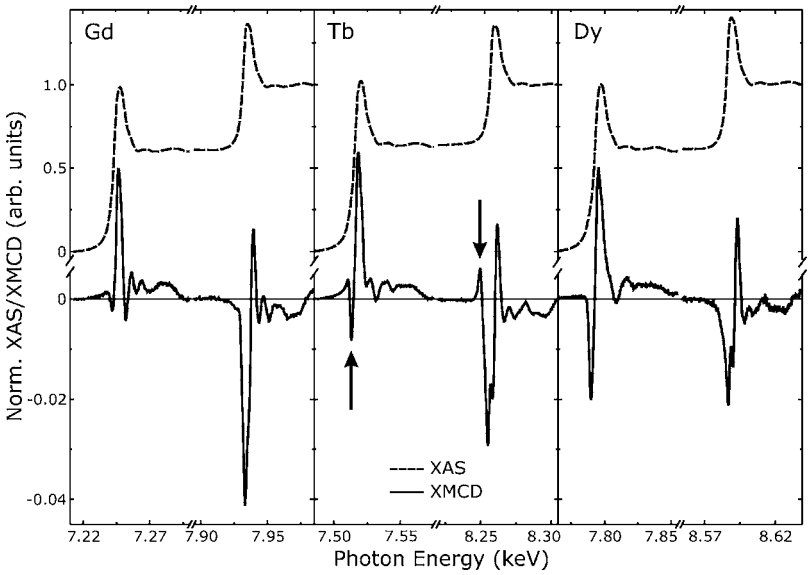

FIG. 1. Normalized XAS (dashed line) and XMCD (solid line) as measured at the $L_{2,3}$ edges of Gd ($T=10$ K, $\mu_0 H=3$ T), Tb ($T=4$ K, $\mu_0 H=7$ T), and Dy ($T=5$ K, $\mu_0 H=5$ T). The y scale for the XAS is given above the axis break, the y scale for the XMCD below. The arrows in the case of Tb as an example mark the $E2$ contributions.

the c axis for Gd, the b axis for Tb, and the a axis for Dy are aligned perpendicular to the surface. In the cases of Tb and Dy these correspond to the crystallographic easy axis of magnetization in bulk material.[16,17] For bulk Gd the crystallographic easy axis would be on a cone around the c axis.[17,18] However, all three samples exhibit a huge shape anisotropy aligning the magnetization parallel to the surface of the sample. Therefore, a field of up to 7 T is applied to overcome the shape anisotropy and align the magnetization perpendicular to the surface during the measurements at normal incidence of the x-rays.

The measurements were carried out at the ID12 beamline at the ESRF in Grenoble, France via fluorescence detection.[19–21] The magnetic field H with $\mu_0 H \leq 7$ T was applied along the beam direction. The XMCD signals were obtained from the difference of the x-ray absorption coefficients $\Delta\mu(E)=\mu^+(E)-\mu^-(E)$ for parallel (μ^+) and antiparallel (μ^-) orientation of the photon helicity and the magnetic field. The spectra were measured consecutively either by reversing the helicity of the incident beam or by flipping the magnetic field. Furthermore, the magnetization $M(H)$ was recorded to determine the field at which the samples are fully saturated.

Figure 1 shows the spin-averaged x-ray absorption spectra (XAS) (dashed line, y scale above break) and the XMCD (solid line, y scale below break) of the three elements Gd, Tb, and Dy at low temperature. The XAS are normalized to a total edge jump of 1. The size of the XMCD is given according to this normalized scale. Since the two edges are well separated in energy they have been measured individually with a high density of data points to clearly identify all the spectral fine structure in the XMCD. The L_3 edge to L_2 edge step ratio is displayed as measured in a long scan with a lower density of data points including both edges. Although the difference in the absorption spectra for the two helicities $\mu^+(E)$ and $\mu^-(E)$ can hardly be made out by eye (not shown in Fig. 1), clear XMCD spectra can be determined. With an energy resolution $\Delta E/E \sim 10^{-4}$ an experimental broadening of somewhat below 1 eV can be expected allowing to identify the detailed spectroscopic features.

The focus is now turned to the details in the temperature-dependent XMCD spectra of the three elements as plotted in Fig. 2. The spectra have been measured in a range from low temperature T up to where the transition from the ferromagnetic to the paramagnetic state occurs. In zero magnetic field Tb and Dy show a helical magnetic phase for $T_C < T < T_N$ which, however, is suppressed in our measurements by the applied magnetic field.

The relative intensities of the different spectral features vary as temperature changes. At different photon energies different temperature dependencies of the XMCD are observed. This becomes, for example, prominent at the L_2 edge of Dy where at $T=185$ K the two peaks of the double structure have the same intensity whereas at $T=5$ K one peak is only approximately half the size of the other one. Thus, for the rare-earth elements Gd, Tb, and Dy, the temperature dependence is more complex than for the $3d$ FMs Fe, Co, and Ni, for example. If only $E1$ transitions occur, the XMCD is proportional to the magnetization—the XMCD scales in intensity with the magnetization as a function of the temperature without changing its line shape. For $E2$ transitions, the XMCD is expected to have a different temperature dependence than the magnetization.[22] Normalizing the temperature-dependent XMCD spectra to the magnetization therefore reveals in which energy range $E2$ transitions contribute to the XMCD. The XMCD spectra normalized to the reduced magnetization $M(T)/M_0$ are shown in Fig. 3 in the relevant energy range close to the edges. For all three elements the deviation from pure scaling with $M(T)$ occurs at the low energy side of the edges where the $E2$ transitions are expected to be prominent (see below).

III. ANALYSIS AND SIMULATION

To support the interpretation of the measured XMCD spectra at low temperatures, complementary theoretical investigations were performed. As a first step the spin-dependent electronic potentials of Gd, Tb, and Dy were determined in a self-consistent way within the framework of the local spin-density approximation (LSDA) to spin-density

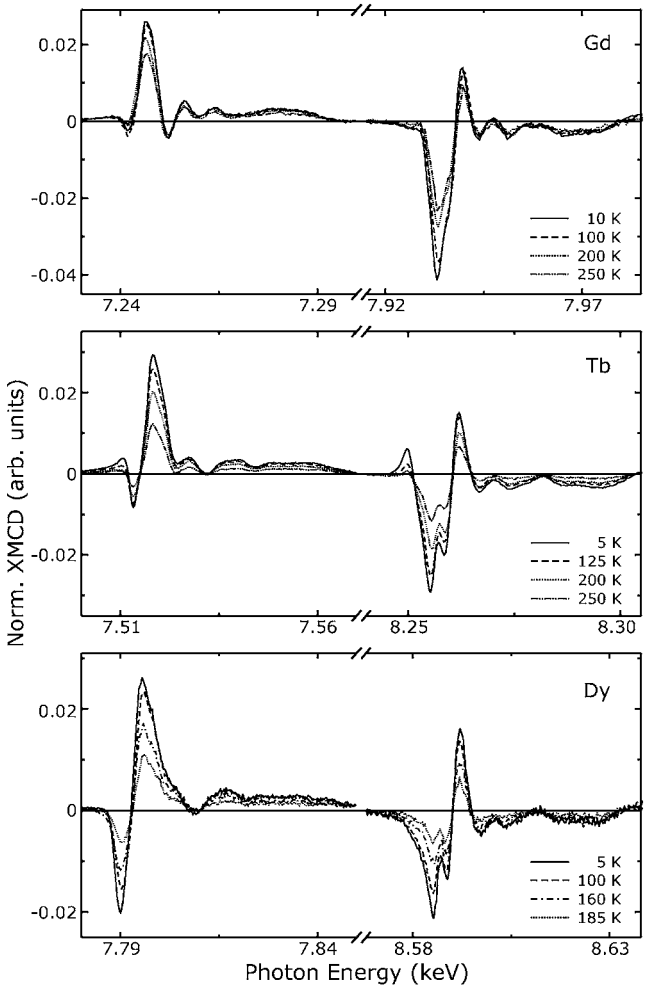

FIG. 2. Temperature-dependent XMCD at the $L_{2,3}$ edges of Gd, Tb, and Dy. The y scale is given according to the corresponding XAS which is normalized to unity (see Fig. 1). To overcome the shape anisotropy and to align the magnetization along the natural direction of easy magnetization, a magnetic field is applied with $\mu_0 H=7$ T for Tb and $\mu_0 H=5$ T for Dy at all temperatures. For Gd the field was reduced from $\mu_0 H=3$ T at $T=10$ K to $\mu_0 H=2.8$ T at $T=100$ K, $\mu_0 H=2.5$ T at $T=200$ K, and $\mu_0 H=2$ T at $T=250$ K.

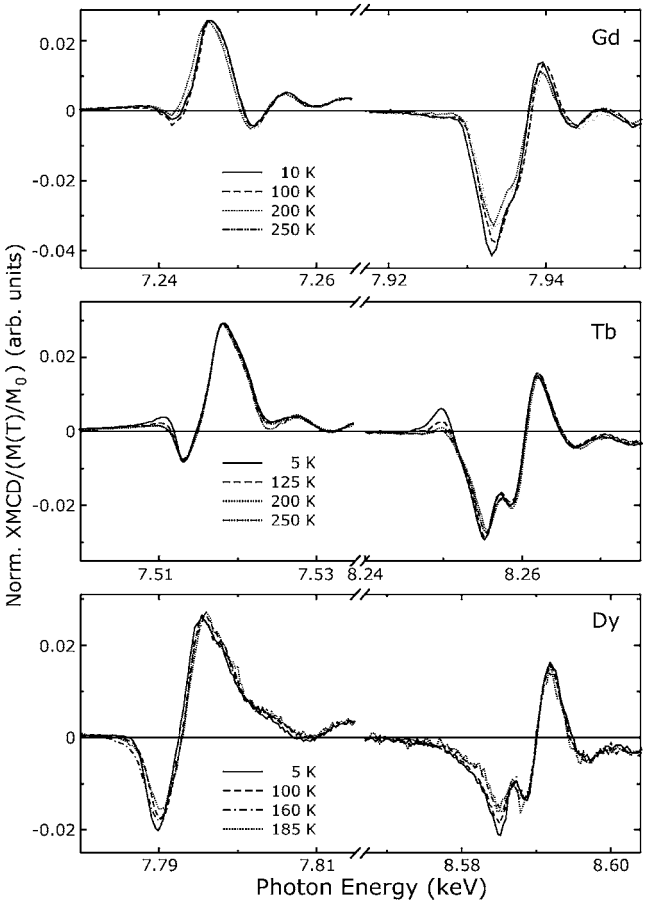

FIG. 3. XMCD spectra normalized to the reduced magnetization $M(T)/M_0$ at the corresponding measuring temperature.

functional theory.[23] In a subsequent step the XAS and XMCD spectra were calculated using a fully relativistic version of the multiple scattering or KKR (Korringa-Kohn-Rostoker) formalism.[1,24] Due to the symmetry of the investigated systems, there is no interference of the $E1$ and $E2$ contributions, i.e., dipolar and quadrupolar, respectively, to the spectra. Accordingly, they could be evaluated separately. Due to the selection rules and the weight given by the radial matrix elements [1] the $E1$ and $E2$ partial spectra stem primarily from $p \rightarrow d$ and $p \rightarrow f$ transitions. As the relative position of the final d and f states is in general not well reproduced by calculations based on plain LSDA, because of an insufficient treatment of correlation effects, the $E1$ and $E2$ partial spectra are in general misaligned. This problem can be further enhanced by core hole effects.[25] We have therefore shifted the $E2$ spectra in energy with respect to the $E1$ spectra but kept their amplitudes unchanged. Note that in a previous theoretical work on the $L_{2,3}$ edges of Gd it was necessary to apply a similar procedure as the $E1$ partial spectra were calculated within the framework of LSDA, while the $E2$ partial spectra were calculated using an atomic description.[6] Furthermore, one should note that this necessary relative shift of the $E1$ and $E2$ partial spectra supplies a very stringent benchmark for the development of an improved and coherent description of correlation effects that goes beyond LSDA. The resulting theoretical XMCD spectra for the $E1$ and $E2$ transitions (dashed and dotted lines, respectively) are shown in Fig. 4(a). In Fig. 4(b) the total calculated XMCD spectra (dashed-dotted lines) are shown in comparison to the experimental ones (solid lines). To allow for this direct comparison with experiment a suitable complex self-energy has been assumed for the calculations to represent finite lifetime effects.[26] To account for the finite apparative resolution an additional broadening of the theoretical spectra was done applying a Gaussian broadening with a width of 1 eV.

As one can see in Fig. 4(b) the resulting theoretical XMCD spectra reproduce the various details of the experimental spectra rather well. In particular the double peak structure at the L_2 edge of Tb and Dy that could be resolved in experiment was confirmed by the calculations. In the case of Gd the second L_2 peak at higher photon energy is not clearly split off but leads to a shoulder in the measured spectrum. The calculations clearly demonstrate that at low photon energies, i.e., at the edges, the $E2$ contributions are opposite

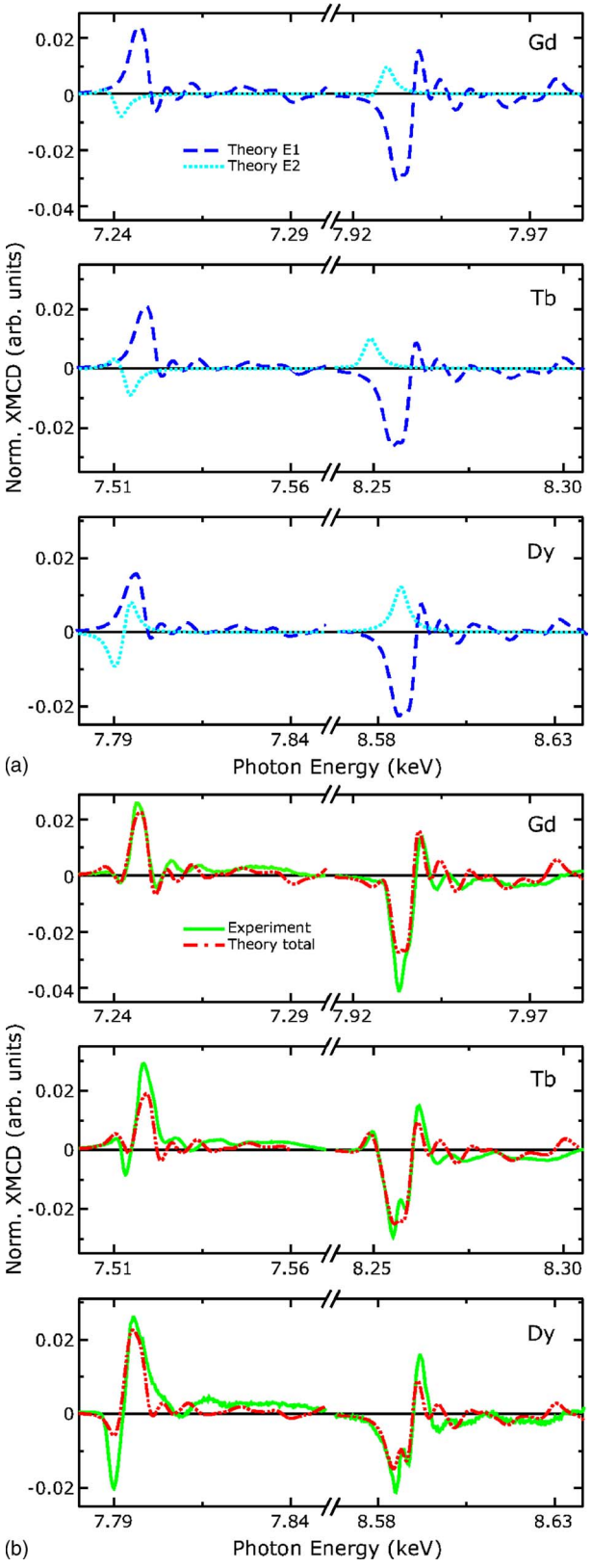

FIG. 4. (Color online) (a) Calculated $E1$ and $E2$ contributions to the XMCD spectra of Gd, Tb, and Dy. (b) Comparison of the measured XMCD spectra at low temperature to the total spectra obtained from calculations.

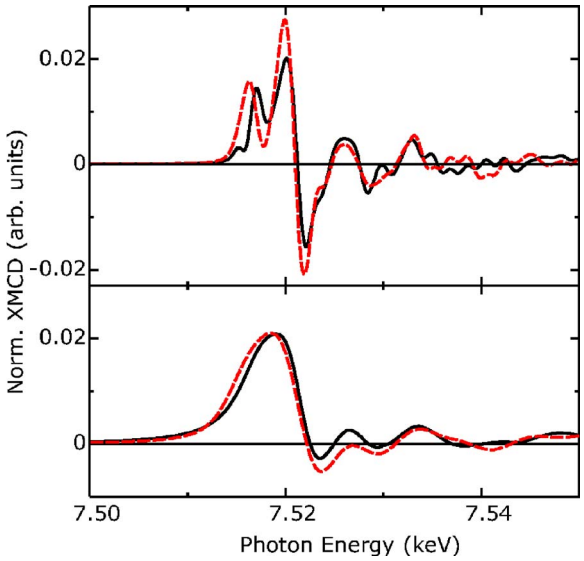

FIG. 5. (Color online) Calculated XMCD at the L_3 edge of Tb as an example including spin-orbit coupling in the final states (solid line) and without spin-orbit coupling in the final states (dashed line). Top, without experimental broadening; bottom, with an experimental broadening of 1 eV.

in sign compared to the dominating $E1$ contributions in all three cases. As a consequence the structure of the XMCD spectra around the edges is therefore strongly influenced by the $E2$ contribution. For the L_2 edge of Gd and Dy, the $E2$ contribution strongly overlaps with the $E1$ contribution. Accordingly, the influence of the $E2$ contribution is hard to be seen in the experimental spectra, but could clearly be identified on the basis of the accompanying calculations. Apart from the edge region, the $E2$ partial spectra does not show any further structure. This reflects the fact that the $4f$ states, which are the final states connected with the $E2$ transitions, are well localized in space with a corresponding narrow energy band width.

To achieve a more detailed understanding of the line shape of the XMCD spectra, the influence of the spin-orbit coupling (SOC) for the final states has been investigated by means of model calculations. As we show in Fig. 4 the prominent double structure in the XMCD at the L_2 edge is of dipolar nature ($E1$). Therefore, we analyze only this $E1$ transition in the following. At the L_3 edge this double structure is not detected. This is an effect of the different final states (J,m_J levels) probed at the two edges. To analyze this further, we show the corresponding results for the L_3 edge of Tb as an example in Fig. 5 with and without the SOC included for the final states. Performing the XMCD calculations with the SOC properly included for the final states and a subsequent broadening with a width of 1 eV leads essentially to a single peak structure (Fig. 5, bottom). For the L_2 edge, on the other hand, a double peak structure emerges as in the measured spectrum (see Fig. 4). If the XMCD calculations are performed with suppressed SOC for the final states, the main peak of the L_3 XMCD spectrum gets slightly broader and shifted (Fig. 5, bottom, dashed line). The impact of the SOC for the final states gets more obvious if the broadening, that was meant to represent the finite apparative resolution, is

omitted. Figure 5 (top) clearly shows that the double peak structure is present for both calculations, i.e., for the SOC for the final states on and off. With the SOC included, the separation of the two peaks is obviously smaller and the intensity of the second peak is strongly removed. Due to the various matrix elements involved at the L_3 edge, spectra are by far dominated by $2p_{3/2} \rightarrow 5d_{5/2}$ transitions, other transitions being less important. Switching off the SOC for the final states obviously suppresses the spectral differences between these transitions that make the most important contributions to the XMCD spectra shown in Fig. 5. This explains why a clear double structure in the $E1$ contribution at the $L2$ edge is revealed (Fig. 2) whereas basically a broad peak is detected at the L_3 edge. The reason for this difference is just due to the different J, m_J levels probed at the respective edges. This demonstrates that for a complete XMCD measurement both edges are required.

IV. SUMMARY

High quality temperature-dependent XMCD spectra have been obtained from measuring single crystals of Gd, Tb, and Dy at their $L_{2,3}$ edges. Interpretation of XMCD at the $L_{2,3}$ edges of rare-earth elements is more complicated than for $3d$ transition metals. The localized magnetic $4f$ electrons spin polarize the $5d$ final states ($E1$ transition), but also have a strong radial overlap with the $2p$ initial states. So core hole effects, $p \rightarrow d$, and $p \rightarrow f$ transitions are all intercorrelated. Standard branching ratios, like in XAS and XMCD of $3d$ transition elements, and simple proportionality of bulk magnetization and XMCD intensity are not expected. On the other hand, these experiments will open a new challenge for example to measure in parallel the shell-specific magnetization of $5d$ and the $4f$ band by means of dipolar and quadrupolar contributions. The complex field- and temperature-dependent magnetic properties encountered in rare earths may then be resolved. A first step towards this goal is to combine the details of the experimental fine structure with *ab initio* calculations. The results of our fully relativistic multiple scattering or KKR formalism is in fair agreement with all details of the experimental spectra.

ACKNOWLEDGMENTS

Discussions with A. Ankudinov and J. J. Rehr are acknowledged. The authors thank P. Poulopoulos, G. Ceballos, and N. Jaouen for assistance in the experiments. Support by BMBF (05 KS4 KEB/5) and the ESRF is gratefully acknowledged.

*Corresponding author; Present address: Max-Planck-Institut für Metallforschung, Heisenbergstraße 3, D-70569 Stuttgart, Germany; Electronic address: babgroup@physik.fu-berlin.de; URL http://www.physik.fu-berlin.de/~bab/

†Present address: SSRL, Stanford Linear Accelerator Center, 2575 Sand Hill Road, Menlo Park, California 94025.

[1] H. Ebert, Rep. Prog. Phys. **59**, 1665 (1996).
[2] J. Stöhr, J. Electron Spectrosc. Relat. Phenom. **75**, 253 (1995).
[3] G. Schütz, M. Knülle, R. Wienke, W. Wilhelm, W. Wagner, P. Kienle, and R. Frahm, Z. Phys. B: Condens. Matter **73**, 67 (1988); G. Schütz and Ahlers, Lect. Notes Phys. **466**, 229 (1995).
[4] B. N. Harmon and A. J. Freeman, Phys. Rev. B **10**, 1979 (1974).
[5] P. Carra and M. Altarelli, Phys. Rev. Lett. **64**, 1286 (1990).
[6] P. Carra, B. N. Harmon, B. T. Thole, M. Altarelli, and G. A. Sawatzky, Phys. Rev. Lett. **66**, 2495 (1991).
[7] J. C. Lang, G. Srajer, C. Detlefs, A. I. Goldman, H. König, X. Wang, B. N. Harmon, and R. W. McCallum, Phys. Rev. Lett. **74**, 4935 (1995).
[8] C. Giorgetti, E. Dartyge, C. Brouder, F. Baudelet, C. Meyer, S. Pizzini, A. Fontaine, and R.-M. Galéra, Phys. Rev. Lett. **75**, 3186 (1995).
[9] R. M. Galéra and A. Rogalev, J. Appl. Phys. **85**, 4889 (1999).
[10] F. Garcia, L. C. Sampaio, A. Y. Takeuchi, H. Tolentino, and A. Fontaine, J. Appl. Phys. **87**, 5881 (2000).
[11] J. B. Goedkoop, J. C. Fuggle, B. T. Thole, G. van der Laan, and G. A. Sawatzky, J. Appl. Phys. **64**, 5595 (1988).
[12] H. Wende, Z. Li, A. Scherz, G. Ceballos, K. Baberschke, A. Ankudinov, J. J. Rehr, F. Wilhelm, A. Rogalev, D. L. Schlagel, and T. A. Lograssso, J. Appl. Phys. **91**, 7361 (2002).
[13] H. Wende, Rep. Prog. Phys. **67**, 2105 (2004).
[14] M. Münzenberg, F. Leuenberger, W. Felsch, G. Krill, T. Neisius, S. Pascarelli, and S. Pizzini, Phys. Rev. B **67**, 224431 (2003).
[15] A. L. Ankudinov, J. J. Rehr, H. Wende, A. Scherz, and K. Baberschke, Europhys. Lett. **66**, 441 (2004).
[16] D. E. Hegland, S. Legvold, and F. H. Spedding, Phys. Rev. **131**, 158 (1963).
[17] D. R. Lide, *CRC Handbook of Chemistry and Physics* (CRC Press, Boca Raton, FL, 1995).
[18] W. E. Corner and B. K. Tanner, J. Phys. C **9**, 627 (1975).
[19] J. Goulon, A. Rogalev, C. Gauthier, C. Goulon-Ginet, S. Paste, R. Signorato, C. Neumann, L. Varga, and C. Malgrange, J. Synchrotron Radiat. **5**, 232 (1998).
[20] J. Goulon, A. Rogalev, F. Wilhelm, N. Jaouen, C. Goulon-Ginet, and C. Brouder, J. Phys.: Condens. Matter **15**, S633 (2003).
[21] C. Gauthier, G. Goujon, S. Feite, E. Moguiline, L. Braicovich, N. B. Brookes, and J. Goulon, Physica B **208&209**, 232 (1995).
[22] C. Gioretti, E. Dartyge, S. Pizzini, A. Fontaine, F. Baudelet, C. Brouder, C. Meyer, and F. de Groot, Physica B **208&209**, 777 (1995).
[23] S. H. Vosko, L. Wilk, and M. Nusair, Can. J. Phys. **58**, 1200 (1980).
[24] H. Ebert, Lect. Notes Phys. **535**, 191 (2000).
[25] A. Rogalev and J. Goulon, AIP Conf. Proc. **506**, 336 (2000).
[26] L. W. Roeland, G. J. Cock, F. A. Muller, A. C. Moleman, K. A. McEwen, R. G. Jordan, and D. W. Jones, J. Phys. F: Met. Phys. **5**, L233 (1975).